Atmospheric Brown Carbon on the Tibetan Plateau: Regional Differences in Chemical Composition and Light Absorption Properties

Jianzhong Xu[1], Anusha Priyadarshani Silva Hettiyadura[2], Yanmei Liu[1], Xinghua Zhang[1], Shichang Kang[1,4], Alexander Laskin[2,3]

[1]State Key Laboratory Cryopheric Sciences, Northwest Institute of Eco-Environment and Resources, Chinese Academy of Science, Lanzhou 730000, China

[2]Department of Chemistry, [3]Department of Earth, Atmospheric and Planetary Sciences, Purdue University, West Lafayette, Indiana 47907-2084, United States

[4]CAS Center for Excellence in Tibetan Plateau Earth Sciences, Beijing 100085, China

Corresponding author:

Alexander Laskin (alaskin@purdue.edu) and Jianzhong Xu (jzxu@lzb.ac.cn)

ABSTRACT

~~In this study, f~~Fine particular matter ($PM_{2.5}$) filter samples were collected from two high-altitude remote sites located in the southern (QOMS) and northern (WLG) regions of the Tibetan Plateau (TP) to explore the regional differences in brown carbon (BrC) properties. Chemical differences in BrC composition representative of these two areas were inferred from molecular-level analysis of the $PM_{2.5}$ samples using high-performance liquid chromatography coupled with photodiode array and high-resolution mass spectrometry detectors. The results show that more polar BrC chromophores were abundant in QOMS samples, while contributions from ~~both~~ polar and less polar chromophores were comparable in WLG samples. A higher mass absorption coefficient of BrC was observed at QOMS than at WLG. Strong BrC chromophores in QOMS samples were identified as oxygenated aromatics and nitrophenol compounds, while organosulfate compounds were found in the WLG sample. The results of this study indicate the regional differences on BrC chromophores and provide insights into their sources and chemical processes, which should be considered for predictive understanding and modelling the radiative forcing of aerosol on the TP.

TOC

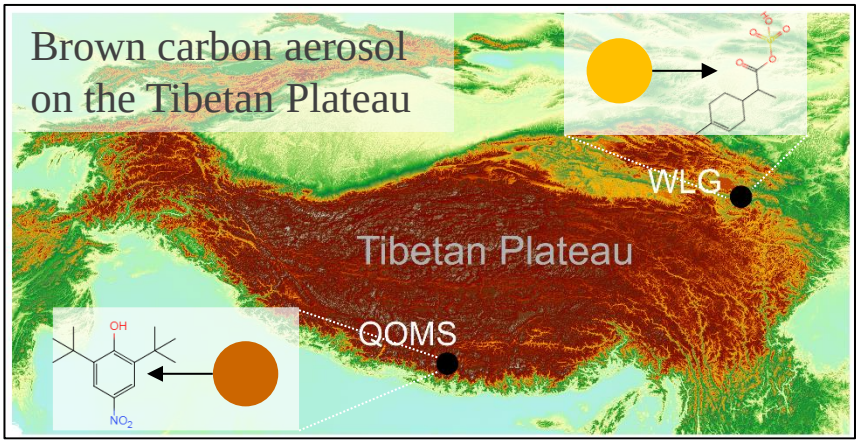

INTRODUCTION

Brown carbon (BrC) is a fraction of atmospheric organic aerosol that absorbs UV-Vis light and is reflected by the yellow to brown color of bulk aerosol samples.[1, 2] BrC is widely distributed in the atmosphere and has significant effects on air quality degradation and radiative forcing of climate.[3, 4] Primary BrC is directly emitted from various sources, while secondary BrC is formed by atmospheric ageing reactions of primary emissions and gases.[2 and references therein] Biomass burning is the main source of primary BrC at the global scale.[5, 6] Oxidation of volatile organic compounds from biogenic and anthropogenic emissions can also lead to the formation of various secondary BrC products.[7-9] The light absorption properties of BrC are further affected by chemical or physical processes of atmospheric ageing such as those driven by photolysis,[10] oxidation,[11] changes in pH,[12, 13] air temperature,[14] and relative humidity.[15] All of these ageing processes contribute to the complex chemical composition and physical properties of BrC.[16]

Light absorption by BrC has a strong wavelength dependency characterized by high values of an absorption Ångström exponent (*AAE*) greater than 2.[1] Therefore, the light absorption by BrC is measured with either online multiwavelength optical instruments (e.g., PASS-3 and aethalometer) [17] or offline UV-vis spectrophotometers after extracting PM filter samples with different solvents.[18, 19] However, the bulk light absorption of BrC does not provide information on the molecular-specific light absorption properties of individual BrC chromophores, which are important for predictive understanding of the sources and evolution of BrC in the atmosphere. Molecular-specific characterization of BrC is commonly performed using an analytical chemistry platform that includes chromatographic separation of BrC compounds with high-performance liquid chromatography (HPLC), characterization of their light absorption with a photodiode array

(PDA) detector, and chemical composition with high-resolution mass spectrometry (HRMS) assisted with soft ionization techniques such as electrospray ionization (ESI) or atmospheric pressure photoionization (APPI).[20] A number of recent studies have adopted this method to characterize BrC compounds from ambient or laboratory-generated samples. For example, Lin, et al. [21]; 2017 and Fleming, et al. [22] analyzed aerosol samples from biomass burning-influenced airmass and found significant contributions from nitroaromatic chromophores. Wang, et al. [23] and Yan, et al. [24] analyzed ambient urban samples in China and found distinct nitrogen- and sulfur-containing BrC as the important light absorbing components in those samples. Lavi, et al. [25] and West, et al. [26] investigated laboratory-generated BrC compounds from biomass burning and ethane fuel combustion, respectively, providing their chemical composition and insights into their formation mechanisms. Recently, Lin, et al. [20] and Hettiyadura, et al. [27] utilized this platform with different ionization techniques to characterize polar and nonpolar BrC chromophores in ambient and laboratory-generated biomass burning samples.

The Tibetan Plateau (TP) has an average altitude of 4000 m a.s.l and a surface area of 2,500,000 km^2, which makes it the highest and largest plateau on Earth. Changes in the climate and atmospheric environment on the TP due to the impact of regional aerosols have been reported in previous studies.[28, 29] These effects are mainly due to the enhanced anthropogenic emissions from rapidly developing industrial activities and fast-growing populations in the surrounding regions and the favorable atmospheric circulation that transports these pollutants to the TP area.[4, 30] Inherent to the wide variability of emission sources, a very complex composition of regional aerosols has been reported in the TP area.[31-33] Of particular note, a high fraction of water soluble BrC has also been reported at the TP.[34-36] Owing to the large surface area of the TP, the chemical

and physical properties of aerosols are substantially different across the northern and southern parts of the TP divided by the Tanggula Mountains (Figure S1). The northern TP is dominated by airmasses from Central Asia and Inland China, while the southern TP is heavily influenced by airmasses arriving from South Asia. In our previous study,[35] we evaluated the overall chemical composition of the $PM_{2.5}$ aerosols at QOMS and WLG sites and assessed the bulk chemical composition and optical properties of water-soluble organic carbon (WSOC) at these two sites using HRMS and UV-Vis spectroscopy, separately. We showed that the light absorption of WSOC at the southern site is greater compared to that at the northern site. Consistently, HRMS analysis showed significant differences in the elemental composition of WSOC at the two sites.[35] In the current study, we utilized HPLC-PDA-HRMS platform to provide molecular composition and the optical properties of individual water-soluble BrC chromophores at the TP for the first time. Furthermore, the current study shed light on sources and formation pathways of the major BrC chromophores at the southern and northern TP, suggesting the regional influences on aerosol chemistry and radiative forcing in the TP.

METHODS AND MATERIALS

Sample collection

Figure S1 shows a regional map and the locations of two high-altitude observatories: the Waliguan Baseline Observatory (WLG) and Qomolangma Station for Atmospheric Environmental Observation and Research (QOMS), where particulate matter ($PM_{2.5}$) filter samples were collected. Explicit details of field sampling at each station have been reported in ~~our~~ previous publications.[32, 33, 35, 37] Briefly, $PM_{2.5}$ filter samples were collected at QOMS during April – May 2016 and at WLG during July 2017, which were representative periods of typical

high aerosol loading episodes at each of the sites. Samples were collected on prebaked quartz filters (47 mm diameter, Tissuquartz 2500 QAT-UP, PALL Life Sciences) with a low volume $PM_{2.5}$ filter sampler (16.7 L min^{-1}, model PQ200, BGI, USA) at two-day frequency. After collection, samples were sealed and kept below 0 °C during transport using a cooler with blue ice and then refrigerated at –20 °C in our laboratory. In this study, a few high mass concentration filters were combined into two samples at WLG (named as WLG1 and WLG2) and three samples at QOMS (named as QOMS1, QOMS2, and QOMS3) for further measurement based on their air mass trajectory analysis (Table S1 and Figure S2).

HPLC-PDA-HRMS

WSOC fractions of aerosol samples were extracted using ultrapure water by sonication, and the obtained extracts were later analyzed using an HPLC-PDA-HRMS platform.[35] The water extract samples were first concentrated and desalted using solid phase extraction (SPE) cartridges (DSC18, Supelco, 3 mL). The procedure for SPE can be found elsewhere~~in our previous paper~~.[35] The solution in acetonitrile of SPE eluent was concentrated using N_2 gas (99.995% purity) and reconstituted in 200 µL dimethylsulfoxide (DMSO) to make a final solution ready for HPLC-PDA-ESI-HRMS analysis. For comparison, one of the WLG samples was also extracted using acetonitrile and concentrated directly using N_2 gas for further analysis using the same WSOC strategy. The using of DMSO was to facilitate dissolving and mixing of the extract with the initial mobile phase solvents that consist of 99.5% (~~V/V~~v/v) water.[20]

Chemical speciation of WSOC components was performed using an HPLC-PDA-(ESI±)-HRMS platform. The platform consists of a Vanquish HPLC system equipped with a PDA detector and

a high-resolution Q-Exactive-HF-X Orbitrap mass spectrometer equipped with an IonMAX ionization source configured as ESI (all modules are from Thermo Scientific, Inc.). The HPLC flow eluted from the column was divided equally between PDA and HRMS for the analysis. Separation was performed on a reversed-phase column (Luna C18(2), 150 × 2 mm^2, 5 µm particles, 100 Å pores, Phenomenex, Inc.). The measurement conditions for the mass spectrometer can be found in our previous paper.[27] UV-Vis absorption spectra were measured using a PDA detector over the wavelength range of 200 – 680 nm. The shift of retention time (RT) between PDA and HRMS signals was determined using three chemical standards (benzoic acid, salicylic acid, and 2,5-dihydroxybenzoic acid) with known UV-vis spectra.

Data Processing

Xcalibur (V4.0, Thermo Scientific) software was used to acquire raw HPLC-PDA-HRMS data. The HPLC-PDA data were further processed using Thermo Xcalibur to produce 3-D maps of light absorption chromatograms and 2-D UV-vis light absorption spectra at selected RT ranges. Chromatographic construction and peak deconvolution of HPLC-HRMS data were performed using MZMine (V2.51, http://mzmine.github.io/), an open-source software. A list of peaks with intensities above the 10 S/N threshold value was extracted for the data analysis. The obtained list of experimental m/z values was processed using home-built Microsoft Excel macros to remove C^{13} isotope peaks and group the peaks into homologous groups based on CH_2 and H_2 using Kendrick mass defects.[38, 39]

Formula assignment for one member in each homologous group identifies all other members of the group. The elemental formulas of ions representative of homologous groups were assigned

using Molecular Formula Calculator (V1.1, https://nationalmaglab.org/user-facilities/icr/icr-software). The chemical constrains for formula assignments were as follows; C>0, H>0, O≥0, 0≤N≤3, 0≤S≤1, and 0≤DBE/n_C≤0.9 (DBE: double-bond equivalent). The DBE was calculated using the following equation: DBE = $c - h/2 + n/2 + 1$,[40] where *c*, *h*, and *n* correspond to the number of carbon, hydrogen, and nitrogen atoms in the formula, respectively. Deprotonated ions $[M-H]^-$ were assigned in negative ion mode; protonated $[M+H]^+$ and sodiated $[M+Na]^+$ ions were assigned in positive ion mode.

Calculation of the mass absorption coefficient (MAC_λ) of BrC

The total MAC_λ corresponding to BrC in each sample was calculated based on HPLC-PDA datasets using the equation shown below:[27]

$$MAC_\lambda(m^2 g^{-1}) = \frac{A_\lambda(\mu AU\ sec) \times F(mL\ min^{-1}) \times \ln(10)}{l(cm) \times m_{inj}(ng) \times 60(sec\ min^{-1}) \times 10}$$

where $A_\lambda(\mu AU\ sec)$ is the area of the HPLC-PDA chromatogram at wavelength λ from 0 – 60 min; $F(mL\ min^{-1})$ is the flow rate of the HPLC; $l(cm)$ is the path length of the PDA optical cell (1 cm); $m_{inj}(ng)$ is the injected mass of a sample calculated by the concentration of water soluble organic carbon (WSOC) and injected volume; ln (10) converts the absorption coefficient from base-10 to natural log; and 10 is the combined conversion factor between different units. The $A_\lambda(\mu AU\ sec)$ of each sample was background subtracted using the light absorption by the LC mobile phase. Note that the mass concentration of WSOC used in the equation can be higher than the actual concentration due to the potential loss of highly polar organic compounds such as small organic acids that might have been lost during the SPE process. The total MAC_λ of each sample was then fractionated to 3 RT ranges (0 – 3 min, 3 – 30 min, and 30 – 60 min) based on the relative light absorption recorded by the PDA in the wavelength range 280 – 500 nm.

RESULTS AND DISCUSSION

Figure 1 shows the 2D heatmaps of the HPLC-PDA chromatograms over retention times of 0 – 60 min for QOMS and WLG samples at the same color scale. There are two notable features for BrC light absorption: (1) stronger light absorption was observed for QOMS samples; (2) more BrC chromophores eluted during the first 30 min of RT in QOMS samples than in WLG samples. These results indicate the presence of more polar BrC chromophores in the QOMS samples than in the WLG samples. To compare the light absorbance at the QOMS and WLG sites quantitively, figure 1 also shows the total MAC_{λ} of water soluble BrC in each sample and their three RT ranges. The ranges of RT used in this study are marked in figure 1 and indicate highly polar (0 – 3 min), polar (3 – 30 min), and moderately/intermediately polar (30 – 60 min) compounds based on the relative absorption of broad classes of BrC components operationally defined for each of the RT ranges. For example, highly polar compounds may be relatively small molecules with multiple -OH and -COOH functional groups, while moderately/intermediately polar compounds may be larger molecules with carbonyl functionality, mostly like oxidized diterpenoids or oxidized lignin products.[41] The average total MAC_{405} value of 0 – 60 min at QOMS (0.35 ± 0.10) was approximately two times higher than that at WLG (0.20 ± 0.08), which was mainly contributed by the higher MAC_{405} values for the 0 – 3 and 3 – 30 min RT regions. The MAC_{405} value of 30 – 60 min at WLG (0.09 ± 0.05) was significantly higher than that at QOMS (0.04 ± 0.02). Correspondingly, the average contribution of $MAC_{280\text{-}400}$ during 30 – 60 min at WLG was higher than that at QOMS (30% vs. 11%). These results further suggest the relatively higher contribution of less polar BrC chromatophores was presented at WLG than QOMS. The extraction using acetonitrile for the same WLG sample (WLG2_ACN) indeed showed an enhanced MAC_{405} value (0.11 vs. 0.09) during 30 – 60 min and higher contributions

of $MAC_{280\text{-}400}$ during the same RT period (33% vs. 25%, Figure 1) compared to WLG2. The indexes of atomic oxygen-to-carbon (O/C), hydrogen-to-carbon (H/C), and aromaticity index (AI) calculated based on assigned formulas for these two sites show an increasing trend for AI and H/C and a decreasing trend for O/C with RT (Figure S3), which are consistent with the non-polar compounds eluted at longer RT in reversed-phase LC.

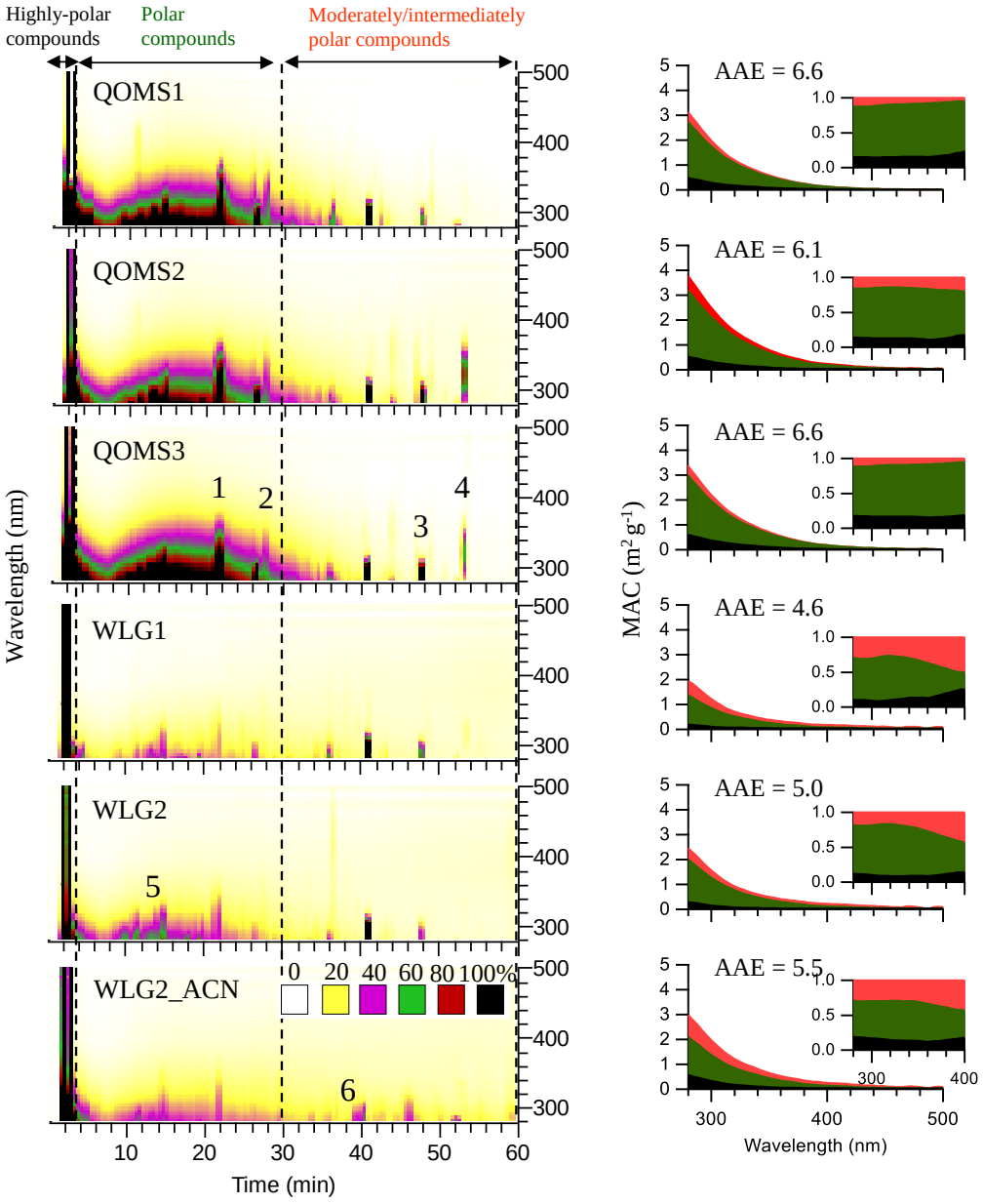

Figure 1. HPLC-PDA 2D heatmap chromatograms recorded for QOMS and WLG samples are shown in the left panel. Vertical dashed lines group PDA features into three RT regions. Six light absorption peaks were marked (four for QOMS3, one for WLG2, and one for WLG2_ACN) and an unmarked peak with RT at ~40 min was likely an impurity in the system. The right panel indicates *MAC* values of water-soluble BrC with contributions fractionated between three broadly defined classes of chemical components (highly polar, polar, and moderately polar) associated with each of three RT ranges. The inserts indicate the relative contributions of the three classes to the total *MAC*. *AAE* values were calculated in the wavelength range of 300 – 400 nm.

Figure 2 shows MAC_{405} values of BrC determined for QOMS and WLG samples mapped in the *AAE* vs. $\log_{10}MAC_{405\ nm}$ space along with four BrC classes suggested by Saleh.[42] The BrC of all samples presented here corresponds to the weak BrC (W-BrC) class. This result is comparable with the results of BrC reported previously (gray symbols in Figure 2) for other TP field sites (marked in Figure S1). The large error bars in previous datasets are likely a result of seasonal variations. For example, the result from the pre-monsoon period at NamCo is close to the result of QOMS with higher MAC_{405} values, while the result from the monsoon period at NamCo is close to the result of WLG with a lower MAC_{405} value.[34] Because of the distinct seasonal variations in sources of aerosols arriving at the TP,[43-45] these results suggest different abundances of BrC chromophores during different seasons and locations on the TP. The southern sites during the non-monsoon period were impacted by regional biomass burning emissions, and they had higher *MAC* values, while the northern sites during the monsoon period were impacted by emissions from inland China.[35] Higher *MAC* and *AAE* values were observed for the WLG sample

extracted in acetonitrile, suggesting abundant water insoluble BrC components. In addition, the position of BrC from the WLG sample is also close to that of snow samples collected from Western China [46] in recent years, supporting their similar BrC properties and sources.

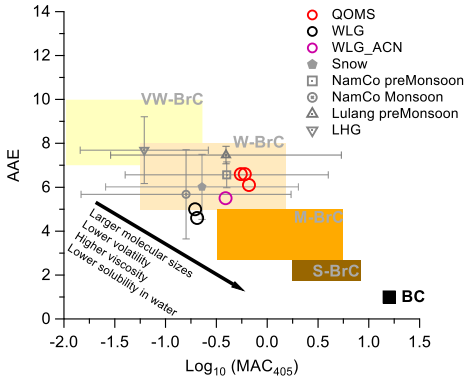

Figure 2. Optical properties of BrC mapped in the *AAE*-log$_{10}$*MAC*$_{405}$ space following the approach of Saleh [42]. Shaded areas indicate "very weakly (VW)", "weakly (W)", "moderately (M)", and "strongly (S)" absorbing BrC classes. Black squares indicate black carbon (BC), and colored circles show the optical properties of the QOMS and WLG samples. Gray markers indicate BrC from the TP and West China reported in previous studies [34, 46] and unpublished data. The calculation of *AAE* for all datasets is based on the same wavelength range of 300-400 nm.

Figures 3a and b show ESI-MS spectra of species eluted over the entire 3 – 60 min period and in each of two RT regions of 3 – 30 min and 30 – 60 min, respectively. Overall, the QOMS and WLG samples show the appearance of the most abundant peaks below 300 Da. Additional peaks between 400 and 700 Da in positive mode appear in the WLG samples, while they are not observable in the QOMS samples. The larger molecules observed in the WLG sample are consistent with the relatively abundant less polar molecules observed in the light absorption measurement. This can also be illustrated by the average formula composition and molecular weight (MW) calculated for each of the MS spectra, i.e., $C_{15.63}H_{21.6}O_{2.43}N_{0.69}S_{0.21}$ (MW = 264.4 Da) and $C_{17.43}H_{23.62}O_{2.64}N_{0.59}S_{0.30}$ (MW = 292.9 Da) in ESI+ mode, for QOMS and WLG, respectively. Figure 3c shows the averaged molecular composition for each case. The total MS was dominated by CHO and CHON category formulas in the QOMS and WLG samples (>65%), but relatively higher fractions of CHOS formulas were also observed in the WLG sample (20% vs. 13% on two mode average). For each RT period, higher contributions of N- and S-containing formulas were observed during 3 – 30 min RT for all the samples consistent with their high polarity, while higher contributions of CHO formulas and less N- and S-containing formulas were observed during 30 – 60 min RT, which were potentially reduced species owing to their less polarity. Similar molecular compositions were also found for the potential BrC components inferred from the diagrams of DBE vs. n_c plotted for all identified species and those eluted during each of two RT periods (Figure S4).

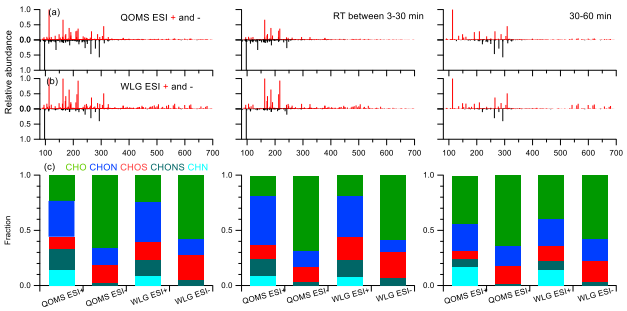

Figure 3. ESI(+) and ESI(–) mass spectra of WSOC components eluting over entire and fractional retention times (RT) shown for (a) QOMS and (b) WLG samples, respectively. (c) The corresponding fractions of formulas assigned in ESI(+) versus ESI(–) ionization modes for combined QOMS and WGL samples.

Since a few stronger light absorption chromophores were observed in QOMS and WLG samples with distinct peaks in the HPLC-PDA chromatograms (marked with numbered legends in the left panel of Figure 1), the molecular composition and their potential sources were elucidated in detail by combining HPLC-HRMS and HPLC-PDA data based on the method of Lin et al.[21] Note that peaks 1 to 4 were from QOMS samples, peak 5 was from water extraction on WLG2, and peak 6 was from acetonitrile extraction on the same WLG2 (Figure 1). The peak selection was based on the subtraction of the 2D heatmap of the QOMS sample from WLG or WLG2_ACN from WLG2 (Figure S5). Figure S6 also shows the UV-Vis spectra for these peaks from PDA chromatograms. The plausible formulas and structure for these six peaks are shown in Table 1,

and their potential sources are discussed below. Peak 1 is assigned to $C_7H_8NO_4$ (i.e., methyl 2-nitrobenzoate), which is a likely product of ethylbenzene/NOx and was observed from biomass burning influenced air mass in other studies.[7, 47, 48] The comparison of the UV-Vis spectra between PDA and $C_7H_8NO_4$ supports this identification (Figure S6). The neutral formula for peak 2 is $C_{18}H_{20}O_3$, which is consistent with ketolimononaldehyde (KLA, $C_9H_{14}O_3$) or its isomers.[49] Peak 3 is assigned to $C_{15}H_{22}O_2$, which has been found in other studies.[50-52] Considering on its UV-Vis spectrum, this compound is assigned to 3,5-di-tert-butyl-4-hydroxybenzaldehyde (Figure S6). Williams, et al. [52] suggested that this compound could originate from the oxidation of biogenic volatile organic compounds (VOCs) or anthropogenic VOCs. The BrC chromophore associated with peak 4 is $C_{14}H_{21}NO_3$, and it was detected in both ESI(+) and ESI(–) modes. This compound is likely 2,6-di-tert-butyl-4-nitrophenol based on the similarity of their UV-Vis spectra (Figure S6). This compound is commonly formed by reactions of nitrogen oxides and biomass burning OA.[51] Peak 5 is assigned with formular $C_{10}H_{16}O_5S$, which may be related to reactive uptake of biogenic volatile organic compounds (BVOCs) in the presence of acidic sulfate aerosol.[53] Recently, Fleming, et al. [54] identified this chromophore by evaporating the products of the ozonolysis of D-limonene in the presence of sulfuric acid. A high influence of anthropogenic emissions with a high contribution of sulfate in the northern TP is frequently observed during summer periods.[33] The neutral formula for peak 6 is $C_{16}H_{20}O_5$, which is possibly a product of di-n-butyl phthalate.[55] The partitioning coefficient (XlogP3) for these BrC molecule (Table 1), an index of hydrophobic parameter increased with the RT, indicating higher hydrophobicity of the BrC chromophores eluted at longer RT.[56] Overall, three of the six major BrC features assigned consist of CHO with a relatively lower oxygen number (2-5). Only peaks 1, 4 and 5 were assigned to nitrogen- and sulfur-containing BrC. All of these major BrC

chromophores are either known oxidation products of biomass burning OA or SOA derived from biogenic VOCs (QOMS)[37] or SOA derived from anthropogenic emissions influenced by BVOCs (WLG).

Overall, based on the results of HPLC-PDA-HRMS analysis, chemical differences in BrC composition were elucidated for aerosol samples collected at QOMS and WLG located in the southern and northern areas of the TP, respectively. Our results indicate BrC chromophores at the QOMS site were mainly related to biomass burning emission, while at the WLG site they were more influenced by anthropogenic emission source. Reported observations are useful for evaluating the regional difference on aerosol chemistry and radiative forcing.

ASSOCIATED CONTENT

Supporting Information

The Supporting Information is available at xxx.

Details on filter samples used in the study (Table S1), location map for two sampling sites in this study and other comparing data sites on the Tibetan Plateau (Figure S1), cluster analysis of 72h air back trajectories at each site (Figure S2), variation of metrics of assigned molecular with retention time (Figure S3), potential brown carbon identified through plots of DBE vs. number of carbon atoms (n_C) (Figure S4), subtraction of PDA data for QOMS and WLG samples (Figure S5), and UV-Vis spectra of 7 peaks marked in the 2-D PDA chromatogram (Figure S6).

AUTHOR INFORMATION

Corresponding Authors

Alexander Laskin – Department of Chemistry; Department of Earth, Atmospheric and Planetary Sciences, Purdue University, West Lafayette, Indiana 47907-2084, United States; orcid.org/0000-0003-2989-5189

Email: alaskin@purdue.edu

Jianzhong Xu – State Key Laboratory Cryopheric Sciences, Northwest Institute of Eco-Environment and Resources, Chinese Academy of Science, Lanzhou 730000, China; orcid.org/0000-0002-9933-1744

Email: jzxu@lzb.ac.cn

Authors

Anusha Priyadarshani Silva Hettiyadura – Department of Chemistry, Purdue University, West Lafayette, Indiana 47907-2084, United States

Yanmei Liu, Xinghua Zhang, Shichang Kang – State Key Laboratory Cryopheric Sciences, Northwest Institute of Eco-Environment and Resources, Chinese Academy of Science, Lanzhou 730000, China

Notes

The authors declare no competing financial interest.

Acknowledgements. We thank for the assistance by field campaign team and staff of QOMS and WLG stations. This research was supported by grants from the National Natural Science Foundation of China (41977189, 41771079), and the Key Laboratory of Cryospheric Sciences Scientific Research Foundation (SKLCS-ZZ-2021). APSH and AL acknowledge support from

the US Department of Energy's (DOE) Atmospheric System Research program, Office of Biological and Environmental Research (OBER), award DE-SC0021977.

REFERENCES:

(1) Andreae, M. O.; Gelencsér, A. Black carbon or brown carbon? The nature of light-absorbing carbonaceous aerosols. *Atmos. Chem. Phys.* **2006,** *6* (10), 3131-3148.
(2) Laskin, A.; Laskin, J.; Nizkorodov, S. A. Chemistry of Atmospheric Brown Carbon. *Chem. Rev.* **2015,** *115* (10), 4335-4382.
(3) Jo, D. S.; Park, R. J.; Lee, S.; Kim, S. W.; Zhang, X. A global simulation of brown carbon: implications for photochemistry and direct radiative effect. *Atmos. Chem. Phys.* **2016,** *16* (5), 3413-3432.
(4) Zhang, R.; Wang, Y.; He, Q.; Chen, L.; Zhang, Y.; Qu, H.; Smeltzer, C.; Li, J.; Alvarado, L. M. A.; Vrekoussis, M.; Richter, A.; Wittrock, F.; Burrows, J. P. Enhanced trans-Himalaya pollution transport to the Tibetan Plateau by cut-off low systems. *Atmos. Chem. Phys.* **2017,** *17* (4), 3083-3095.
(5) Washenfelder, R. A.; Attwood, A. R.; Brock, C. A.; Guo, H.; Xu, L.; Weber, R. J.; Ng, N. L.; Allen, H. M.; Ayres, B. R.; Baumann, K.; Cohen, R. C.; Draper, D. C.; Duffey, K. C.; Edgerton, E.; Fry, J. L.; Hu, W. W.; Jimenez, J. L.; Palm, B. B.; Romer, P.; Stone, E. A.; Wooldridge, P. J.; Brown, S. S. Biomass burning dominates brown carbon absorption in the rural southeastern United States. *Geophys. Res. Lett.* **2015,** *42* (2), 653-664.
(6) Tian, J.; Wang, Q.; Ni, H.; Wang, M.; Zhou, Y.; Han, Y.; Shen, Z.; Pongpiachan, S.; Zhang, N.; Zhao, Z.; Zhang, Q.; Zhang, Y.; Long, X.; Cao, J. Emission Characteristics of Primary Brown Carbon Absorption From Biomass and Coal Burning: Development of an Optical Emission Inventory for China. *J. Geophys. Res. Atmos.* **2019,** *124* (3), 1879-1893.
(7) Xie, M.; Chen, X.; Hays, M. D.; Lewandowski, M.; Offenberg, J.; Kleindienst, T. E.; Holder, A. L. Light Absorption of Secondary Organic Aerosol: Composition and Contribution of Nitroaromatic Compounds. *Environ. Sci. Technol.* **2017,** *51* (20), 11607-11616.
(8) Desyaterik, Y.; Sun, Y.; Shen, X.; Lee, T.; Wang, X.; Wang, T.; Collett Jr., J. L. Speciation of "brown" carbon in cloud water impacted by agricultural biomass burning in eastern China. *J. Geophys. Res. Atmos.* **2013,** *118* (13), 7389-7399.
(9) Nguyen, T. B.; Lee, P. B.; Updyke, K. M.; Bones, D. L.; Laskin, J.; Laskin, A.; Nizkorodov, S. A. Formation of nitrogen- and sulfur-containing light-absorbing compounds accelerated by evaporation of water from secondary organic aerosols. *J. Geophys. Res. Atmos.* **2012,** *117* (D1).
(10) Lee, H. J.; Aiona, P. K.; Laskin, A.; Laskin, J.; Nizkorodov, S. A. Effect of Solar Radiation on the Optical Properties and Molecular Composition of Laboratory Proxies of Atmospheric Brown Carbon. *Environ. Sci. Technol.* **2014,** *48* (17), 10217-10226.
(11) Sareen, N.; Moussa, S. G.; McNeill, V. F. Photochemical Aging of Light-Absorbing Secondary Organic Aerosol Material. *J. Phys. Chem. A.* **2013,** *117* (14), 2987-2996.
(12) Phillips, S. M.; Bellcross, A. D.; Smith, G. D. Light Absorption by Brown Carbon in the Southeastern United States is pH-dependent. *Environ. Sci. Technol.* **2017,** *51* (12), 6782-6790.
(13) Lin, P.; Bluvshtein, N.; Rudich, Y.; Nizkorodov, S. A.; Laskin, J.; Laskin, A. Molecular Chemistry of Atmospheric Brown Carbon Inferred from a Nationwide Biomass Burning Event. *Environ. Sci. Technol.* **2017,** *51* (20), 11561-11570.
(14) Rincón, A. G.; Guzmán, M. I.; Hoffmann, M. R.; Colussi, A. J. Thermochromism of Model Organic Aerosol Matter. *J. Phys. Chem.* **2010,** *1* (1), 368-373.
(15) Song, C.; Gyawali, M.; Zaveri, R. A.; Shilling, J. E.; Arnott, W. P. Light absorption by secondary organic aerosol from α-pinene: Effects of oxidants, seed aerosol acidity, and relative humidity. *J. Geophys. Res. Atmos.* **2013,** *118* (20), 11,741-11,749.
(16) Hems, R. F.; Schnitzler, E. G.; Liu-Kang, C.; Cappa, C. D.; Abbatt, J. P. D. Aging of Atmospheric Brown Carbon Aerosol. *ACS Earth Space Chem.* **2021,** *5* (4), 722-748.

(17) Lack, D. A.; Langridge, J. M. On the attribution of black and brown carbon light absorption using the Ångström exponent. *Atmos. Chem. Phys.* **2013,** *13* (20), 10535-10543.
(18) Chen, Y.; Bond, T. C. Light absorption by organic carbon from wood combustion. *Atmos. Chem. Phys.* **2010,** *10* (4), 1773-1787.
(19) Hecobian, A.; Zhang, X.; Zheng, M.; Frank, N.; Edgerton, E. S.; Weber, R. J. Water-Soluble Organic Aerosol material and the light-absorption characteristics of aqueous extracts measured over the Southeastern United States. *Atmos. Chem. Phys.* **2010,** *10* (13), 5965-5977.
(20) Lin, P.; Fleming, L. T.; Nizkorodov, S. A.; Laskin, J.; Laskin, A. Comprehensive Molecular Characterization of Atmospheric Brown Carbon by High Resolution Mass Spectrometry with Electrospray and Atmospheric Pressure Photoionization. *Anal. Chem.* **2018,** *90* (21), 12493-12502.
(21) Lin, P.; Aiona, P. K.; Li, Y.; Shiraiwa, M.; Laskin, J.; Nizkorodov, S. A.; Laskin, A. Molecular Characterization of Brown Carbon in Biomass Burning Aerosol Particles. *Environ. Sci. Technol.* **2016,** *50* (21), 11815-11824.
(22) Fleming, L. T.; Lin, P.; Roberts, J. M.; Selimovic, V.; Yokelson, R.; Laskin, J.; Laskin, A.; Nizkorodov, S. A. Molecular composition and photochemical lifetimes of brown carbon chromophores in biomass burning organic aerosol. *Atmos. Chem. Phys.* **2020,** *20* (2), 1105-1129.
(23) Wang, X.; Hayeck, N.; Brüggemann, M.; Abis, L.; Riva, M.; Lu, Y.; Wang, B.; Chen, J.; George, C.; Wang, L. Chemical Characteristics and Brown Carbon Chromophores of Atmospheric Organic Aerosols Over the Yangtze River Channel: A Cruise Campaign. *J. Geophys. Res. Atmos.* **2020,** *125* (16), e2020JD032497.
(24) Yan, C.; Zheng, M.; Desyaterik, Y.; Sullivan, A. P.; Wu, Y.; Collett Jr., J. L. Molecular Characterization of Water-Soluble Brown Carbon Chromophores in Beijing, China. *J. Geophys. Res. Atmos.* **2020,** *125* (15), e2019JD032018.
(25) Lavi, A.; Lin, P.; Bhaduri, B.; Carmieli, R.; Laskin, A.; Rudich, Y. Characterization of Light-Absorbing Oligomers from Reactions of Phenolic Compounds and Fe(III). *ACS Earth Space Chem.* **2017,** *1* (10), 637-646.
(26) West, C. P.; Hettiyadura, A. P. S.; Darmody, A.; Mahamuni, G.; Davis, J.; Novosselov, I.; Laskin, A. Molecular Composition and the Optical Properties of Brown Carbon Generated by the Ethane Flame. *ACS Earth Space Chem.* **2020,** *4* (7), 1090-1103.
(27) Hettiyadura, A. P. S.; Garcia, V.; Li, C.; West, C. P.; Tomlin, J.; He, Q.; Rudich, Y.; Laskin, A. Chemical Composition and Molecular-Specific Optical Properties of Atmospheric Brown Carbon Associated with Biomass Burning. *Environ. Sci. Technol.* **2021,** *55* (4), 2511-2521.
(28) Lau, K. M.; Kim, M. K.; Kim, K. M. Asian summer monsoon anomalies induced by aerosol direct forcing: the role of the Tibetan Plateau. *Clim. Dyn.* **2006,** *26* (7), 855-864.
(29) Ramanathan, V.; Ramana, M. V.; Roberts, G.; Kim, D.; Corrigan, C.; Chung, C.; Winker, D. Warming trends in Asia amplified by brown cloud solar absorption. *Nature* **2007,** *448* (7153), 575-578.
(30) Lüthi, Z. L.; Škerlak, B.; Kim, S. W.; Lauer, A.; Mues, A.; Rupakheti, M.; Kang, S. Atmospheric brown clouds reach the Tibetan Plateau by crossing the Himalayas. *Atmos. Chem. Phys.* **2015,** *15* (11), 6007-6021.
(31) Xu, J.; Zhang, Q.; Shi, J.; Ge, X.; Xie, C.; Wang, J.; Kang, S.; Zhang, R.; Wang, Y. Chemical characteristics of submicron particles at the central Tibetan Plateau: insights from aerosol mass spectrometry. *Atmos. Chem. Phys.* **2018,** *18* (1), 427-443.
(32) Zhang, X.; Xu, J.; Kang, S.; Liu, Y.; Zhang, Q. Chemical characterization of long-range transport biomass burning emissions to the Himalayas: insights from high-resolution aerosol mass spectrometry. *Atmos. Chem. Phys.* **2018,** *18* (7), 4617-4638.
(33) Zhang, X.; Xu, J.; Kang, S.; Zhang, Q.; Sun, J. Chemical characterization and sources of submicron aerosols in the northeastern Qinghai–Tibet Plateau: insights from high-resolution mass spectrometry. *Atmos. Chem. Phys.* **2019,** *19* (11), 7897-7911.
(34) Zhang, Y.; Xu, J.; Shi, J.; Xie, C.; Ge, X.; Wang, J.; Kang, S.; Zhang, Q. Light absorption by water-soluble organic carbon in atmospheric fine particles in the central Tibetan Plateau. *Environ. Sci. Pollut. Res.* **2017,** *24* (26), 21386-21397.
(35) Xu, J.; Hettiyadura, A. P. S.; Liu, Y.; Zhang, X.; Kang, S.; Laskin, A. Regional Differences of Chemical Composition and Optical Properties of Aerosols in the Tibetan Plateau. *J. Geophys. Res. Atmos.* **2020,** *125* (1), e2019JD031226.
(36) Zhu, C.-S.; Qu, Y.; Huang, H.; Chen, J.; Dai, W.-T.; Huang, R.-J.; Cao, J.-J. Black Carbon and Secondary Brown Carbon, the Dominant Light Absorption and Direct Radiative Forcing Contributors of the Atmospheric Aerosols Over the Tibetan Plateau. *Geophys. Res. Lett.* **2021,** *48* (11), e2021GL092524.
(37) An, Y.; Xu, J.; Feng, L.; Zhang, X.; Liu, Y.; Kang, S.; Jiang, B.; Liao, Y. Molecular characterization of organic aerosol in the Himalayas: insight from ultra-high-resolution mass spectrometry. *Atmos. Chem. Phys.* **2019,** *19* (2), 1115-1128.

(38) Roach, P. J.; Laskin, J.; Laskin, A. Higher-Order Mass Defect Analysis for Mass Spectra of Complex Organic Mixtures. *Anal. Chem.* **2011,** *83* (12), 4924-4929.
(39) Eckert, P. A.; Roach, P. J.; Laskin, A.; Laskin, J. Chemical Characterization of Crude Petroleum Using Nanospray Desorption Electrospray Ionization Coupled with High-Resolution Mass Spectrometry. *Anal. Chem.* **2012,** *84* (3), 1517-1525.
(40) McLafferty, F. W.; Tureček, F.; Turecek, *Interpretation of mass spectra*. University Science Books: 1993.
(41) Xu, J.; Brodu, N.; Wang, J.; Abdelouahed, L.; Taouk, B. Chemical characteristics of bio-oil from beech wood pyrolysis separated by fractional condensation and water extraction. *Journal of the Energy Institute* **2021,** *99*, 186-197.
(42) Saleh, R. From Measurements to Models: Toward Accurate Representation of Brown Carbon in Climate Calculations. *Curr. Pollut. Rep.* **2020,** *6* (2), 90-104.
(43) Cong, Z.; Kang, S.; Kawamura, K.; Liu, B.; Wan, X.; Wang, Z.; Gao, S.; Fu, P. Carbonaceous aerosols on the south edge of the Tibetan Plateau: concentrations, seasonality and sources. *Atmos. Chem. Phys.* **2015,** *15* (3), 1573-1584.
(44) Xu, J.; Wang, Z.; Yu, G.; Qin, X.; Ren, J.; Qin, D. Characteristics of water soluble ionic species in fine particles from a high altitude site on the northern boundary of Tibetan Plateau: Mixture of mineral dust and anthropogenic aerosol. *Atmos. Res.* **2014,** *143* (0), 43-56.
(45) Zhu, C.-S.; Cao, J.-J.; Huang, R.-J.; Shen, Z.-X.; Wang, Q.-Y.; Zhang, N.-N. Light absorption properties of brown carbon over the southeastern Tibetan Plateau. *Sci. Total Environ.* **2018,** *625*, 246-251.
(46) Zhou, Y.; West, C. P.; Hettiyadura, A. P. S.; Niu, X.; Wen, H.; Cui, J.; Shi, T.; Pu, W.; Wang, X.; Laskin, A. Measurement report: Molecular composition, optical properties, and radiative effects of water-soluble organic carbon in snowpack samples from northern Xinjiang, China. *Atmos. Chem. Phys.* **2021,** *21* (11), 8531-8555.
(47) Xie, M.; Chen, X.; Hays, M. D.; Holder, A. L. Composition and light absorption of N-containing aromatic compounds in organic aerosols from laboratory biomass burning. *Atmos. Chem. Phys.* **2019,** *19* (5), 2899-2915.
(48) Wang, Y.; Hu, M.; Lin, P.; Tan, T.; Li, M.; Xu, N.; Zheng, J.; Du, Z.; Qin, Y.; Wu, Y.; Lu, S.; Song, Y.; Wu, Z.; Guo, S.; Zeng, L.; Huang, X.; He, L. Enhancement in Particulate Organic Nitrogen and Light Absorption of Humic-Like Substances over Tibetan Plateau Due to Long-Range Transported Biomass Burning Emissions. *Environ. Sci. Technol.* **2019,** *53* (24), 14222-14232.
(49) Nguyen, T. B.; Laskin, A.; Laskin, J.; Nizkorodov, S. A. Brown carbon formation from ketoaldehydes of biogenic monoterpenes. *Faraday Discuss.* **2013,** *165* (0), 473-494.
(50) Roskamp, M. J. Characterization of Secondary Organic Aerosol Precursors Using Two-Dimensional Gas Chromatography with Time of Flight Mass Spectrometry (GC×GC/TOFMS). Master of Science (M.S.), Portland State University, Doctoral dissertation, 2013.
(51) Williams, B. J.; Goldstein, A. H.; Kreisberg, N. M.; Hering, S. V. In situ measurements of gas/particle-phase transitions for atmospheric semivolatile organic compounds. *Proc. Natl. Acad. Sci. U.S.A.* **2010,** *107* (15), 6676-6681.
(52) Williams, B. J.; Goldstein, A. H.; Millet, D. B.; Holzinger, R.; Kreisberg, N. M.; Hering, S. V.; White, A. B.; Worsnop, D. R.; Allan, J. D.; Jimenez, J. L. Chemical speciation of organic aerosol during the International Consortium for Atmospheric Research on Transport and Transformation 2004: Results from in situ measurements. *J. Geophys. Res. Atmos.* **2007,** *112* (D10).
(53) Nguyen, Q. T.; Christensen, M. K.; Cozzi, F.; Zare, A.; Hansen, A. M. K.; Kristensen, K.; Tulinius, T. E.; Madsen, H. H.; Christensen, J. H.; Brandt, J.; Massling, A.; Nøjgaard, J. K.; Glasius, M. Understanding the anthropogenic influence on formation of biogenic secondary organic aerosols in Denmark via analysis of organosulfates and related oxidation products. *Atmos. Chem. Phys.* **2014,** *14* (17), 8961-8981.
(54) Fleming, L. T.; Ali, N. N.; Blair, S. L.; Roveretto, M.; George, C.; Nizkorodov, S. A. Formation of Light-Absorbing Organosulfates during Evaporation of Secondary Organic Material Extracts in the Presence of Sulfuric Acid. *ACS Earth Space Chem.* **2019,** *3* (6), 947-957.
(55) Tintaru, A.; Labed, V.; Charles, L. Structural Characterisation of Degradation Products Formed upon Di-n-Butyl Phthalate Radiolysis by High-Performance Liquid Chromatography Electrospray Tandem Mass Spectrometry. *Eur. J. Mass Spectrom.* **2010,** *16* (5), 595-603.
(56) Cheng, T.; Zhao, Y.; Li, X.; Lin, F.; Xu, Y.; Zhang, X.; Li, Y.; Wang, R.; Lai, L. Computation of Octanol−Water Partition Coefficients by Guiding an Additive Model with Knowledge. *J. Chem. Inf. Model.* **2007,** *47* (6), 2140-2148.

Table 1. Summary strong BrC features identified in HPLC-PDA plots. XlogP3 obtained from pubchem.ncbi.nlm.nih.gov is shown as a measure of hydrophobicity.

Peak#	Mass measured	RT (min)	ESI mode (+/–)	Neutral formula	Suggested Structure	DBE	XlogP3*
1	180.0294	22.24	–	$C_7H_8NO_4$	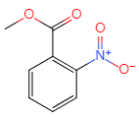	6	1.7
2	285.1481	26.83	+	$C_{18}H_{20}O_3$	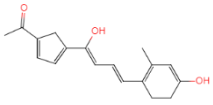	9	/
3	235.1691	48.24	+	$C_{15}H_{22}O_2$	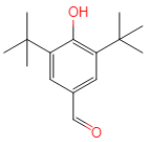	5	4.4
4	252.1592	53.60	+/–	$C_{14}H_{21}NO_3$	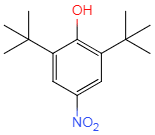	4	4.7
5	247.0644	13.63	–	$C_{10}H_{16}O_5S_1$	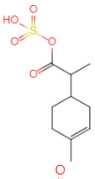	3	/
6	315.1200	39.5	+	$C_{16}H_{20}O_5$	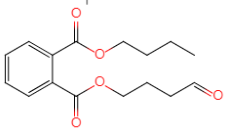	7	/

* XlogP3 is the logarithmic value of octanol-water partitioning coefficient (P) of a compound computed by XLogP3 3.0 (PubChem release 2021.05.07); a higher XlogP3 indicates higher hydrophobicity.[56]